Developmental Biology 443 (2018) 127–136

Contents lists available at ScienceDirect

Developmental Biology

journal homepage: www.elsevier.com/locate/developmentalbiology

Cas9 ribonucleoprotein complex allows direct and rapid analysis of coding and noncoding regions of target genes in *Pleurodeles waltl* development and regeneration

Miyuki Suzuki[a], Toshinori Hayashi[b,*], Takeshi Inoue[c], Kiyokazu Agata[c,d], Miki Hirayama[d], Miyuzu Suzuki[e], Shuji Shigenobu[e], Takashi Takeuchi[b], Takashi Yamamoto[a], Ken-ichi T. Suzuki[a,e,**]

[a] *Department of Mathematical and Life Sciences, Graduate School of Science, Hiroshima University, 1-3-1 Kagamiyama, Higashi-Hiroshima, Hiroshima 739-8526, Japan*
[b] *School of Life Sciences, Faculty of Medicine, Tottori University, 86 Nishi-cho, Yonago, Tottori 683-8503, Japan*
[c] *Graduate Course in Life Science, Gakushuin University, 1-5-1 Mejiro, Toshima-ku, Tokyo 171-8588, Japan*
[d] *Department of Biophysics, Graduate School of Science, Kyoto University, Kitashirakawa-Oiwake, Kyoto 606-8502, Japan*
[e] *National Institute for Basic Biology, Nishigonaka 38, Myodaiji, Okazaki, Aichi 444-8585, Japan*

ARTICLE INFO

Keywords:
CRISPR-Cas9
Genome editing
Newt
Regeneration

ABSTRACT

Newts have remarkable ability to regenerate their organs and have been used in research for centuries. However, the laborious work of breeding has hampered reverse genetics strategies in newt. Here, we present simple and efficient gene knockout using Cas9 ribonucleoprotein complex (RNP) in *Pleurodeles waltl*, a species suitable for regenerative biology studies using reverse genetics. Most of the founders exhibited severe phenotypes against each target gene (*tyrosinase*, *pax6*, *tbx5*); notably, all *tyrosinase* Cas9 RNP-injected embryos showed complete albinism. Moreover, amplicon sequencing analysis of Cas9 RNP-injected embryos revealed virtually complete biallelic disruption at target loci in founders, allowing direct phenotype analysis in the F_0 generation. In addition, we demonstrated the generation of *tyrosinase* null F_1 offspring within a year. Finally, we expanded this approach to the analysis of noncoding regulatory elements by targeting limb-specific enhancer of sonic hedgehog, known as the zone of polarizing activity regulatory sequence (ZRS; also called MFCS1). Disruption of ZRS led to digit deformation in limb regeneration. From these results, we are confident that this highly efficient gene knockout method will accelerate gene functional analysis in the post-genome era of salamanders.

1. Introduction

Newt shows various unique biological properties such as remarkable regenerative abilities in multiple organs (Parish et al., 2007; Barbosa-Sabanero et al., 2012; Inoue et al., 2012; Leone et al., 2015; Tsutsumi et al., 2015; Stocum, 2017), tumor resistance (Seilern-Aspang and Kratochwil, 1962; Oviedo and Beane, 2009), and continuous gonad differentiation (Flament et al., 2009). However, molecular genetic research in newt has been hampered by difficulties in breeding and the lack of a simple and efficient method for gene modification. To overcome this, we recently adopted Iberian ribbed newt *Pleurodeles waltl* as a laboratory newt (Hayashi et al., 2013; Urata et al., 2018). *P. waltl* can be bred easily and reaches sexual maturity in 6 months (male) or 9 months (female); in addition, fertilized eggs can be obtained every 2 weeks throughout the year. Recently, the genomic sequence of *P. waltl* was obtained and edited using clustered regularly interspaced short palindromic repeat (CRISPR)-Cas technology, providing a foundation for comparative genomic and regeneration studies (Elewa et al., 2017).

CRISPR-Cas-based genome editing has been established as an efficient and simple tool for gene disruption in many species and allowed functional investigations in nonmodel organisms. In addition, in urodeles, the effectiveness of CRISPR-Cas has been reported in several studies (Flowers et al., 2014; Fei et al., 2014; Bryant et al.,

* Corresponding author.
** Corresponding author at: Department of Mathematical and Life Sciences, Graduate School of Science, Hiroshima University, 1-3-1 Kagamiyama, Higashi-Hiroshima, Hiroshima 739-8526, Japan.
E-mail addresses: toshih2@tottori-u.ac.jp (T. Hayashi), suzuk107@hiroshima-u.ac.jp (K. T. Suzuki).

https://doi.org/10.1016/j.ydbio.2018.09.008
Received 23 March 2018; Received in revised form 7 September 2018; Accepted 7 September 2018
Available online 10 September 2018
0012-1606/

2017; Elewa et al., 2017). Recently, it was reported that a premixture of recombinant Cas9 protein and guide RNA (gRNA), which forms a ribonucleoprotein complex (RNP), efficiently introduced mutation in virtually all somatic cells in injected founder embryos in zebrafish, designated as crispants (Burger et al., 2016). We previously demonstrated that Cas9 RNP can effectively introduce gene disruption in *Xenopus tropicalis*, somatic mutation rates of which reached ~ 100% (Sakane et al., 2018).

To develop an effective and simple method of gene disruption in newt, we used Cas9 RNP in *P. waltl* and evaluated the efficiency of

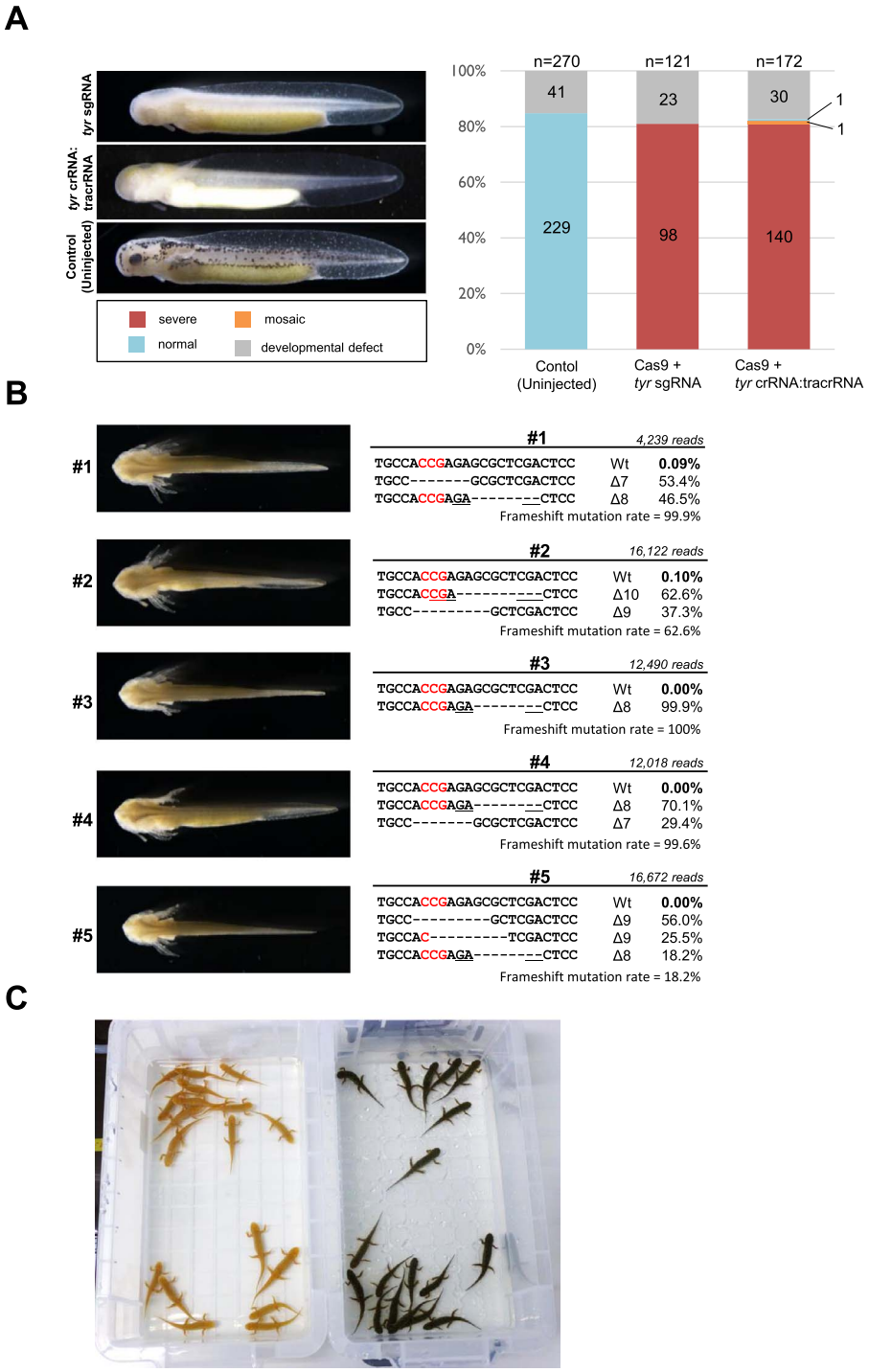

Fig. 1. Targeted gene disruption of *tyrosinase* (*tyr*) in *Pleurodeles waltl* (A) Representative phenotypes of *tyr* gRNAs/Cas9 protein-injected embryos (crispants) and their frequencies. Cas9 protein and sgRNA- (upper panel) or crRNA:tracrRNA-injected embryos (middle panel) showed almost complete albino phenotypes. The two gRNAs have the identical target sequence (Fig. S2). Phenotypes are classified into three groups: severe, complete loss of pigmentation in retina pigmented epithelium (RPE); mosaic, partial loss of pigmentation in RPE; and normal, no alteration of pigmentation. Note that almost all surviving crispants showed a severe albino phenotype. Total and each group's sample sizes (n) are indicated at the top and middle of each graph, respectively. Each value was obtained from two independent experiments. (B) Genotypes of *tyr* crispants analyzed by amplicon sequencing. Representative mutant alleles, their occupancy rates, frameshift mutation rates, and total read counts are shown corresponding to each crispant (#1–5). Deletions are indicated by dashes. Protospacer adjacent motif (PAM) and microhomologous sequences are indicated by red letters and underscores, respectively. Less than 1% of wild-type alleles were found even though over ten thousand reads were sequenced, suggesting the saturation of mutagenesis in the founder. All mutant alleles and their frequencies are listed in Table S1. (C) *tyr* crispant (left) and wild-type (uninjected controls; right) juveniles.

somatic mutations in these crispants using next-generation sequencing. Strikingly, we found extremely high mutation rates that exceeded 99% for each target locus in the analyzed genes, suggesting the potential to expand this approach to high-throughput analysis. Moreover, we demonstrated the generation of F_1 offspring from crispants within a year. Finally, we assessed the effect of this approach on the function of noncoding regulatory elements by targeting limb-specific enhancer of sonic hedgehog (*shh*), known as the zone of polarizing activity regulatory sequence (ZRS; also called MFCS1, Sagai et al., 2005).

2. Results

2.1. Cas9 RNP enabled highly efficient gene disruption in newt

To examine the efficiency of CRISPR-Cas-mediated gene disruption in *P. waltl*, we first targeted *tyrosinase* (*oculocutaneous albinism IA*; *tyr*) involved in melanin synthesis. Upon the injection of Cas9 RNP as proof of principle, we evaluated two types of guide RNA (gRNA) with the same target sequence prepared in different manners (Figs. S1–3). One was *in vitro*-transcribed single guide RNA (sgRNA) using PCR templates and the other was chemically synthesized *trans*-activating CRISPR RNA (tracrRNA) and CRISPR RNA (crRNA). Surprisingly, a week after the injection of Cas9 RNP, both types of gRNA led to nearly complete loss of pigmentation throughout the body in almost all injected embryos (crispants; Fig. 1A). Furthermore, the same severity of phenotype was observed upon injecting other gRNAs targeting the different coding sequences of *tyr* (Fig. S4). Next, to evaluate the efficiency in terms of the somatic mutation rate, amplicon sequencing analysis was performed. Genomic DNA was extracted from the whole body of each crispant (#1–5) and the target genomic locus was amplified and sequenced on a MiSeq platform using a 2× 300-bp paired-end protocol. Even though thousands of reads were analyzed, which may refer to the genotypes of thousands randomly selected cells, almost 100% of alleles were mutated in all analyzed embryos (Fig. 1B, Table S1). Amplicon sequencing also revealed that one to three alleles occupied over 99% of total read counts. We also found a low frameshift mutation rate, but severe phenotypes in #2 and #5 embryos, suggesting the functional importance of the target coding region in *tyr* (Fig. 1B). Dozens of *tyr* crispants were obtained from one experiment; 50 of 70 hatched embryos developed normally and metamorphosed (Fig. 1C).

We previously reported that, by breeding *P. waltl* at a warmer temperature (25–26 °C), the period required for sexual maturation can be shortened to six months in males and nine months in females (Hayashi et al., 2013). *tyr* crispants also showed sex characteristics within several months and females started to spawn from nine months after fertilization under these rearing conditions. The first F_1 offspring were obtained by crossing crispants with each other within a year (Fig. 2A). To confirm the genotype of *tyr* F_1 offspring, genomic DNA was extracted from the tail tip and the target site was sequenced. *tyr* alleles were homozygous, with full albino phenotypes being shown in each clutch (Fig. 2B).

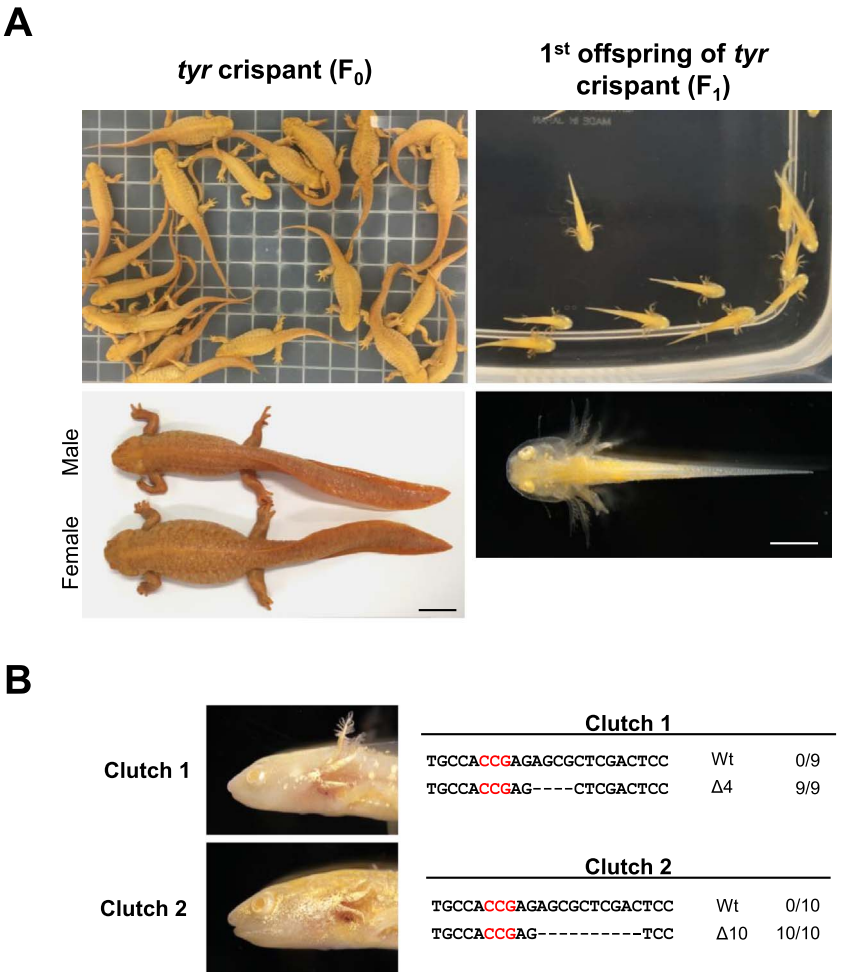

Fig. 2. Generation of F_1 offspring by crossing *tyr* crispants. (A) Sexually mature *tyr* crispants (founders, F_0). From 50 juveniles (3 months postfertilization), 39 adults survived for 17 months and most of them reached sexual maturity within a year. Scale bar = 20 mm. The first F_1 offspring were obtained on 15 Aug, 2017, from the *tyr* crispants (F_0) established on 19 Aug, 2016. Scale bar = 2 mm. (B) Genotypes of *tyr* F_1 offspring from two clutches identified by Sanger sequencing. Deletions are indicated by dashes. The number of clones for each allele is indicated on the right. Sequences represent homozygous mutants in two albino clutches. PAM is indicated by red letters.

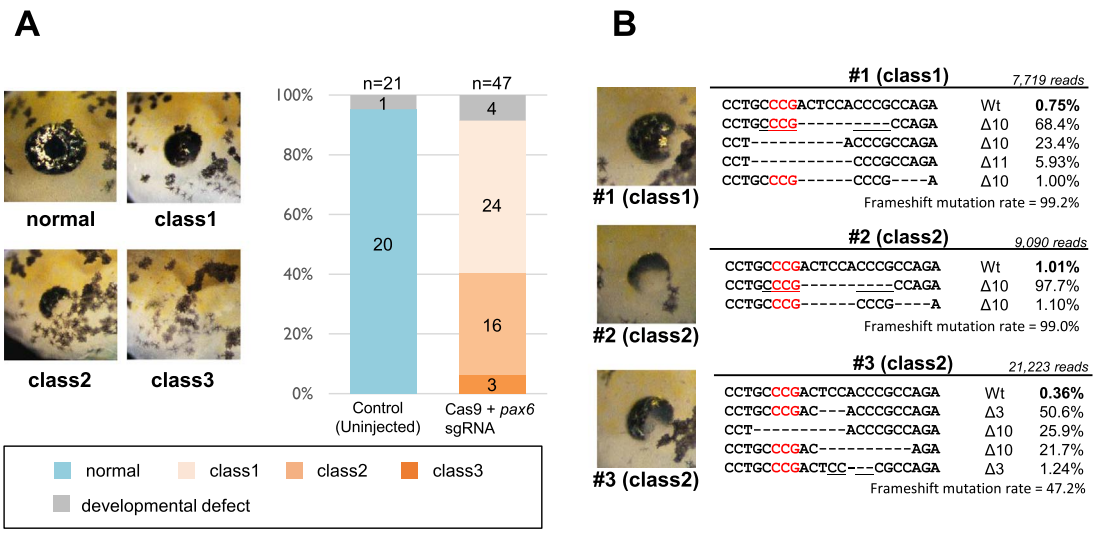

Fig. 3. Targeted gene disruption of *pax6* (A) Representative phenotypes of *pax6* crispant and frequencies of phenotypes from two independent experiments. Phenotypes are classified into four groups, in accordance with a previous report (Yasue et al., 2017). All of the *pax6* crispants showed eye malformation. Total and each group's sample sizes (n) are indicated at the top and middle of each graph, respectively. (B) Genotypes of *pax6* crispants. Representative mutant alleles, their occupancy rates, frameshift mutation rates, and total read counts are shown corresponding to each embryo (#1–3). Deletions are indicated by dashes. PAM and microhomologous sequences are indicated by red letters and underscores, respectively. All mutant alleles and their frequencies are listed in Table S1.

For the next proof-of-principle experiment, we targeted *pax6*, which is involved in eye formation (Suzuki et al., 2013; Yasue et al., 2017). Consistent with previous reports, *pax6* crispants showed eye malformations, for example, small eye (class 1), small eye with partial loss of pigmentation (class 2), or no eye (class 3) (Fig. 3A). Furthermore, all crispants showed eye defects, suggesting the high efficiency of gene disruption by Cas9 RNP, similar to that of *tyr*. The same phenotype was also observed for different sgRNA (Fig. S4). Amplicon sequencing analysis revealed that somatic mutation rates were 99% or higher, with a few different types of mutation occurring, similar to the results for *tyr* (Fig. 3B, Table S1). We found no relationship between the levels of frame shift mutation rates and the severity of the phenotypes, consistent with a previous report on a mouse study (Yasue et al., 2017).

Finally, we also targeted *tbx5*, which is required for forelimb bud formation (Agarwal et al., 2003; Rallis et al., 2003) and heart development (Bruneau et al., 2001; Garrity et al., 2002). *tbx5* crispants had no detectable forelimb buds consistent with previous reports on other vertebrates (Fig. 4A). Moreover, hearts of *tbx5* crispants beat slower than those of wild-type embryos without visible blood flow (Movie S1: beating heart of wild-type larva, Movie S2: beating heart of *tbx5* crispant), indicating heart abnormalities. The same phenotype was also observed in the other crRNA:tracrRNA, which targeted a different coding sequence of *tbx5*, but was never seen in the control groups: the uninjected group and the Cas9 protein and tracrRNA-injected (without *tbx5* crRNA) group (Fig. 4B, Fig. S4). Amplicon sequencing analysis revealed virtually complete biallelic disruption in all analyzed embryos with a few different types of mutation (Fig. 4C).

2.2. ZRS perturbation caused digit deformation during limb regeneration

We next tested whether the use of this Cas9 RNP system can be expanded to the analysis of *cis*-regulatory elements, not only coding sequences. We targeted limb-specific enhancer of *shh*, known as the zone of polarizing activity regulatory sequence (ZRS). ZRS is essential for proper limb development in mouse (Sagai et al., 2005) and recently a 17-bp snake-specific deletion in ZRS was reported (Kvon et al., 2016). This 17-bp sequence is specifically deleted in multiple species of snake and present in limbed tetrapods and fish, and was shown to be able to resurrect the snake ZRS enhancer function in mouse (Kvon et al., 2016). We designed two sgRNAs adjacent to the 17-bp snake-specific deletion site of ZRS in the *P. waltl* genome to excise out this sequence (Fig. 5A, Fig. S5), and co-injected them into one-cell-stage embryos. Regarding limb development, both forelimb and hindlimb of ZRS crispants seemed to develop normally, without limb truncation like in ZRS-deleted mouse (Sagai et al., 2005) and mouse with its original ZRS replaced by snake ZRS (Kvon et al., 2016). Most of the ZRS crispants formed four digits in forelimb, the same as in the wild type, whereas 7 of 33 larvae formed only three digits (Fig. 5B; left column). To investigate this further, we amputated the forelimb of ZRS crispants. Unlike in development, digit formation was severely disrupted in regeneration; specifically, approximately half of ZRS crispants failed to complete regeneration, while wild-type larvae regenerated their digits completely (Fig. 5B; right column). Notably, the formation of one or two digits was seen only in ZRS crispants. We observed an one-digit-regenerated ZRS crispant for 13 months, but it failed to regenerate the other digits at the end of this period (Fig. S6), suggesting that this phenotype reflects impaired regeneration but not delayed regeneration. Genomic DNA was extracted from the amputated limb and genotyped individually for each phenotype (Fig. 5C, Table S1). Entire deletion of the 17-bp sequence did not occur as we expected, even in cases of defective regeneration; however, all analyzed alleles had an insertion or deletion (indel) at the ZRS sgRNA2 cleavage site (Fig. 5C, Table S1). To examine whether ZRS perturbation affected the *shh* expression in regeneration, we quantified *shh* expression in each blastema of ZRS crispants (n = 21) and uninjected siblings (n = 16) using RT-qPCR analysis. As expected, *shh* expression level was significantly lower in ZRS crispants than in the wild type (Fig. 5D).

3. Discussion

We have presented here a highly efficient and simple method of gene knockout in newt by using Cas9 recombinant protein and synthetic crRNA:tracrRNA duplex or *in vitro*-transcribed sgRNA using PCR-based templates to accelerate reverse genetics in newt (Fig. 6). Cas9 recombinant protein is more effective than Cas9 mRNA because it can be active immediately after delivery into human cells and zebrafish eggs (Kim et al., 2014; Burger et al., 2016). As we previously demonstrated in *Xenopus* (Shigeta et al., 2016; Sakane et al., 2018), Cas9 RNP actually achieved highly efficient gene disruption in *P. waltl*, even in the founder generation. Amplicon sequencing analysis of on-

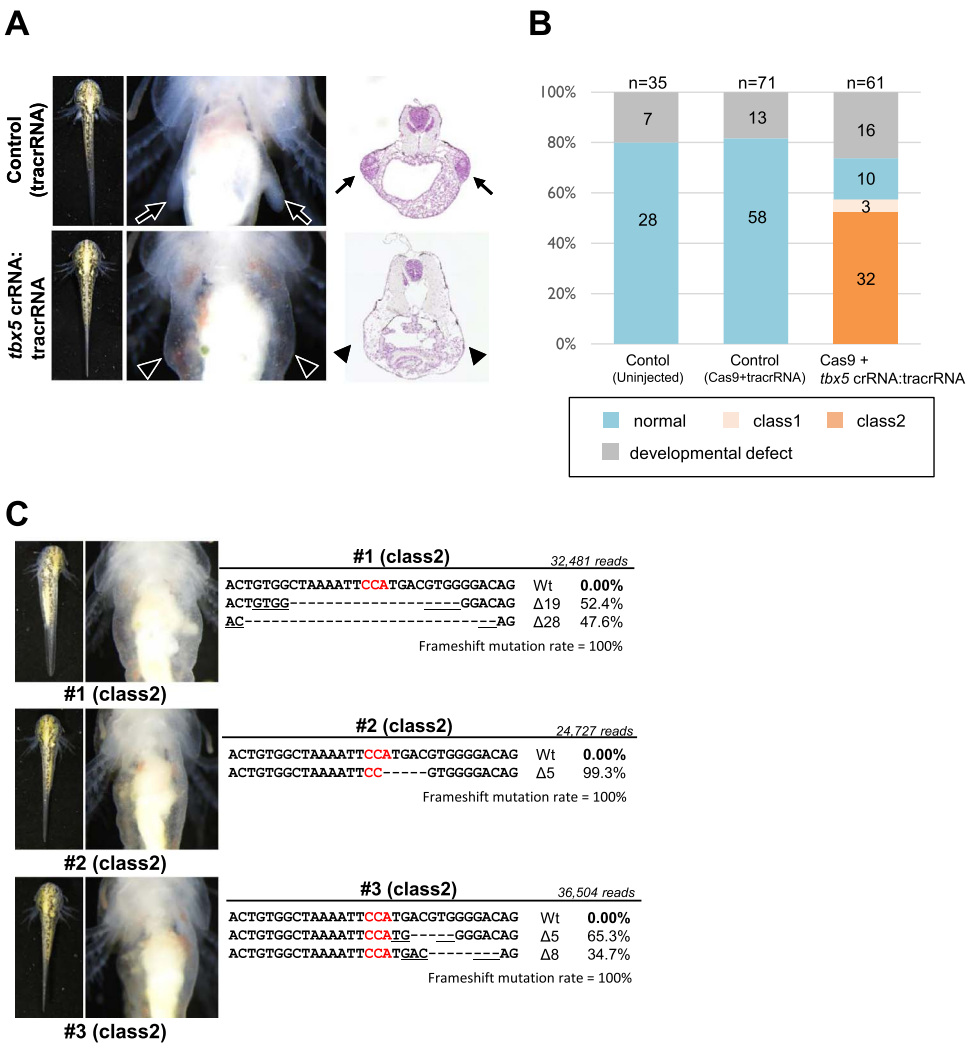

Fig. 4. Targeted gene disruption of *tbx5* (A) A representative phenotype of *tbx5* crispant; dorsal view, ventral view, and cross section through the torso. Arrow and arrowhead indicate limb bud formation in the control and no limb bud formation in the *tbx5* crispant, respectively. (B) Frequencies of phenotypes from two independent experiments. Phenotypes are classified into two groups: class 1, limb defect only; and class 2, limb defect and heart abnormalities. Neither of the control experimental groups, uninjected and Cas9 protein with only tracrRNA injected (without *tbx5* crRNA), showed these phenotypes. (C) Genotypes of *tbx5* crispants. Representative mutant alleles, their occupancy rates, frameshift mutation rates, and total read counts are shown corresponding to each embryo (#1–3). Deletions are indicated by dashes. PAM and microhomologous sequences are indicated by red letters and underscores, respectively. All mutant alleles and their frequencies are listed in Table S1.

target sites revealed saturating somatic mutations in most of the crispants (> 99%), allowing direct phenotype readouts from them (Ablain et al., 2015; Burger et al., 2016; Zuo et al., 2017; Sakane et al., 2018). For this rapid phenotype analysis, the retention of wild-type and various in-frame alleles is a major concern. In *P. waltl*, we found on average fewer than four mutation alleles in crispants exhibiting severe phenotypes. This suggests that somatic mutations caused by Cas9 RNP resulted in saturation after a few initial cleavages. Sanger sequencing analysis of on-target sites also led to the estimation of a low somatic allele count of genome-edited *P. waltl* (Hayashi et al., 2014; Elewa et al., 2017), and we assume that the longer time for the first cleavage in *P. waltl* (5–6 h at 25 °C) would ensure the efficiency of genome editing (Hayashi et al., 2014). Furthermore, we demonstrated the generation of *tyr* F_1 offspring from crispants within a year. Therefore, we are confident that both crispants with saturated mutation and their F_1 progeny will facilitate the functional analysis of genes of interest.

Frameshift mutation disrupts proper translation due to a premature stop codon and nonsense-mediated mRNA decay, so it is the main cause of gene loss of function caused by CRISPR-Cas. The frameshift rates reached 100% in *tbx5* crispants (Fig. 4C); however, they were lower in #2 and #5 *tyr* crispants (Fig. 1B) and #3 *pax6* crispants (Fig. 3B), even though their phenotypes indicated severe loss of function of the target genes. The gRNAs were designed to recognize exon 1 of *tyr* or DNA binding domain in *pax6*, which would be critical for the function of each protein (Suzuki et al., 2013). Therefore, designing gRNAs against the functional domains would contribute to efficient gene loss of function, even if in-frame mutations occur (Burger et al., 2016; Shigeta et al., 2016). We found phenotypic spectrum in *pax6* crispants, as with the previous reports in mouse and *Xenopus* (Suzuki et al., 2013; Yasue et al., 2017). *pax6* is a transcription factor that regulates itself during eye formation. Therefore, its somatic mutation (*e.g.*, various truncated proteins and mosaicism in optic cup and lens placode) may perturb the *pax6* gene network and result in varying degrees of eye malformation. In addition, designing multiple gRNAs to the target gene is also preferable for efficient gene disruption, since it is known that the cleavage activity of programmable nucleases is affected by the chromatin state at the target site (Wu et al., 2014; Kuscu et al., 2014). Actually, phenotype frequencies were shown to vary in a manner dependent on the sequences of gRNAs against a target gene. In our study, at least one gRNA induced a severe phenotype in ~ 80% of embryos when we tested two or three gRNAs

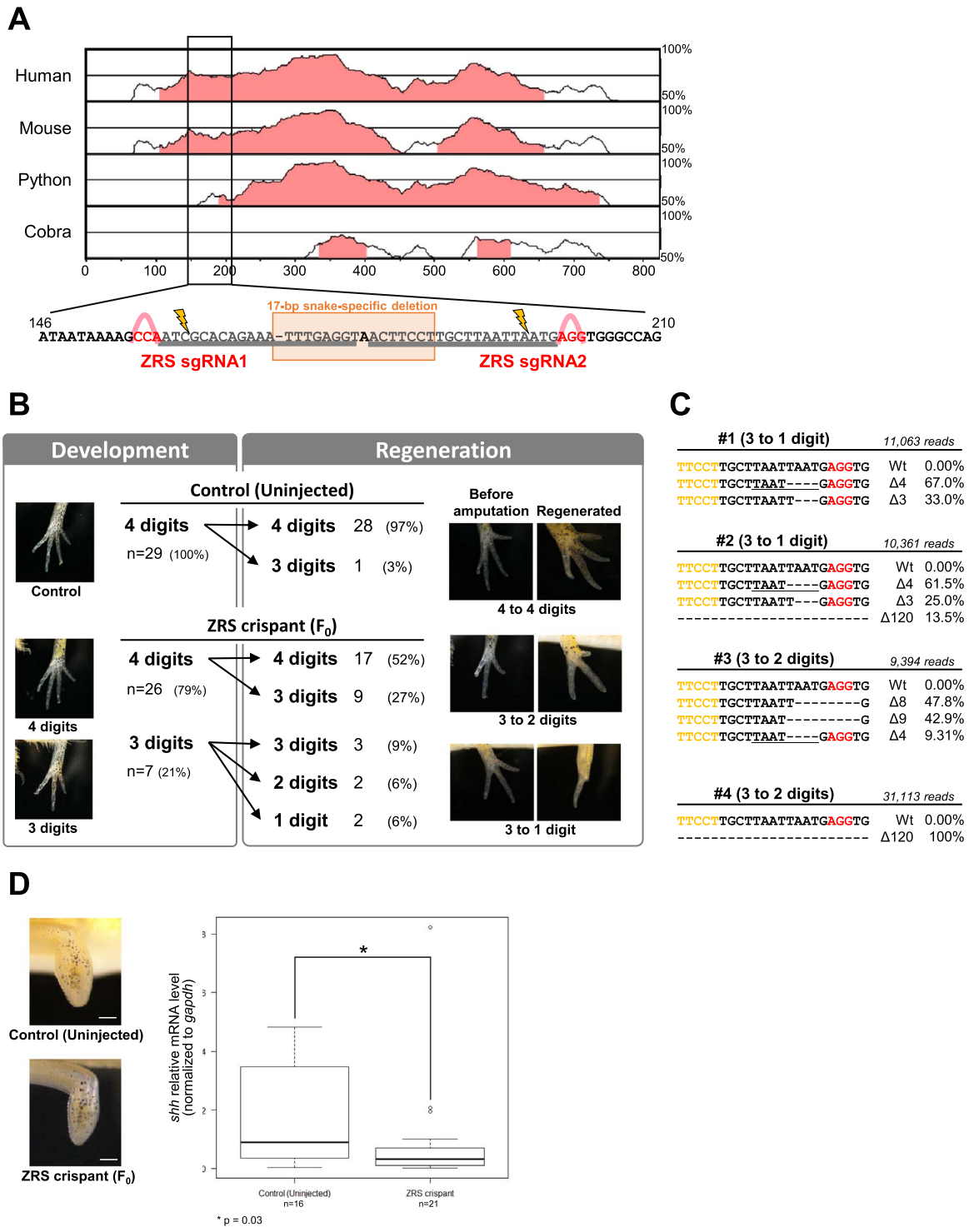

Fig. 5. Targeted *cis*-regulatory element disruption of the limb enhancer of *sonic hedgehog* (A) The VISTA plot of the zone of polarizing activity regulatory sequence (ZRS). The plot shows conserved sequences between *P. waltl* and human, mouse, and snakes (python and cobra). Putative 17-bp snake-specific deletions in *P. waltl* ZRS and sgRNA target sequences are shown below the plot. sgRNA target and PAM sequence are marked in gray and red, respectively. (B) Left column: Phenotypes of ZRS crispants in limb development (1-month postfertilization). Most of the ZRS crispants developed limbs normally and 7 of 33 larvae showed the loss of one digit. Numbers of digits of left forelimbs and their frequencies are shown. Right column: Phenotypes of ZRS crispants in limb regeneration. Unlike in limb development, severe reduction of digit formation was seen. In addition, approximately half of ZRS-disrupted larvae could not regenerate their digits completely. Numbers of regenerated digits and their frequencies are shown. (C) Genotypes of ZRS crispants with severe phenotypes. Genomic DNA was extracted from each amputated limb (#1–4) and the target genomic locus was sequenced. Representative mutant alleles, their occupancy rates, and total read counts are shown. Deletions are indicated by dashes. PAM, part of the 17-bp snake-specific deletion site, and microhomologous sequences are indicated by red and yellow letters, and underscores, respectively. Genotypes of other larvae with moderate phenotypes, all mutant alleles, and their frequencies are listed in Table S1. (D) Quantitative analysis of *shh* expression in regenerating ZRS crispants. Left panel: The left forelimbs were amputated at the middle of the forearm level and regenerating blastemas were collected at 7 days postamputation. Scale bar = 500 μm. Right panel: Boxplot of *shh* mRNA level in each blastema from wild-type (n = 16) and ZRS crispant (n = 21) relative to *gapdh* measured by RT-qPCR. *shh* expression was significantly decreased in ZRS crispant (*: Mann–Whitney *U*-test, p = 0.03).

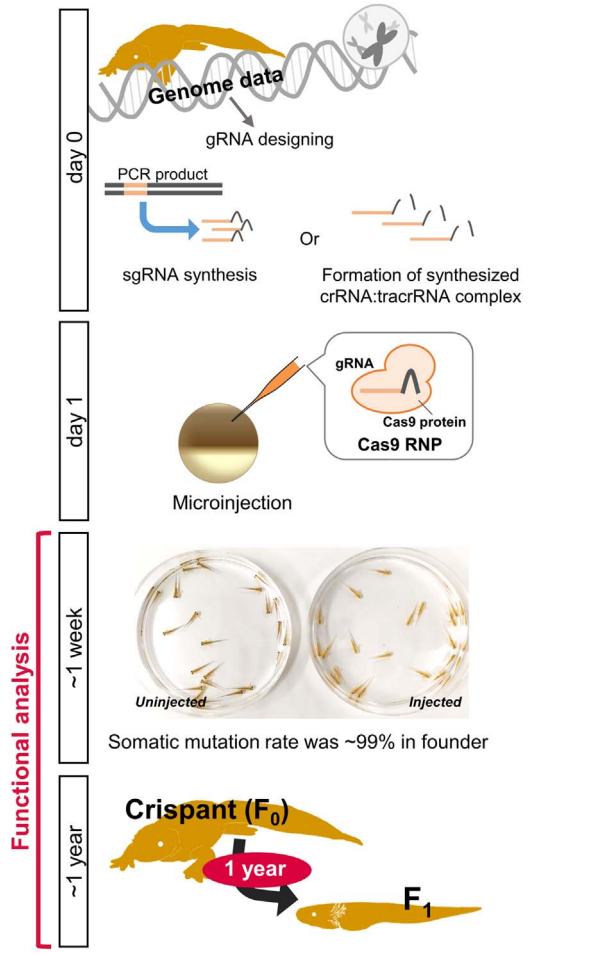

Fig. 6. A schematic diagram of crispants for functional analysis of coding and regulatory regions of *P. waltl* genes.

against each target gene. Moreover, confirming the identical phenotype using multiple gRNAs is one way of avoiding the misreading of phenotypes and obtaining reliable phenotypes due to off-target effects in salamanders, in view of their huge genome size (Fei et al., 2014). Recently, the genome of *P. waltl* has been sequenced (Elewa et al., 2017), so more detailed off-target evaluation can now be applied; for example, candidates of off-target sites can be identified from genome sequence data and unexpected mutations are easily examined by performing a heteroduplex mobility assay on the candidates (Zhu et al., 2014; Shigeta et al., 2016).

Functional assessment of noncoding regulatory elements is important to understand how genes are up- or downregulated in a precise spatiotemporal manner during development and regeneration. The CRISPR-Cas9 system also allows us to investigate their function easily *in vivo*, not only the functions of protein-coding genes (Han et al., 2015; Burger et al., 2016). We designed a pair of gRNAs adjacent to the 17-bp snake-specific deletion site to excise out this sequence; however, they did not remove it. Optimization of the distance of two gRNAs would be needed when using offset gRNAs (Ran et al., 2013), but we were unable to design another gRNA due to the very small region of interest. Even though the deletion of ZRS was only 4–5 bp, it caused severe digit deformation in regeneration. Meanwhile, a large 120-bp deletion was occasionally seen (~ 10%). Such large deletions occur in association with programmable nucleases (Shin et al., 2017): when double-strand breaks at the target site are mainly repaired by the non-homologous end joining (NHEJ) pathway, endogenous nucleases could occasionally create large deletions.

We demonstrated that CRISPR-mediated perturbation of ZRS decreased *shh* mRNA expression and led to defects in digit patterning during regeneration. Similar phenotypes of digit loss were also seen in regenerating limb treated with cyclopamine, a *shh* signaling inhibitor, in a dose-dependent manner (Roy and Gardiner, 2002), supporting the view that the failure of limb regeneration in the ZRS crispant was caused by insufficient reactivation of *shh*. Notably, ZRS-perturbed newts showed variability in their regenerating ability; some of them regenerated their limbs normally, despite possessing similar mutations at the on-target site. Variation of limb phenotype upon ZRS perturbation was also reported to be seen in ZRS 3′-end-deleted mouse (Lettice et al., 2014) and mouse carrying human ZRS (in which the endogenous mouse ZRS had been replaced with human ZRS; Kvon et al., 2016). Even point mutations in ZRS would be a factor that weakens or strengthens *cis–trans* interaction, consequently subtly altering *shh* expression (Williamson et al., 2011; Lettice et al., 2017). This subtle alteration can lead to stochastic variability of phenotypes associated with ZRS mutations (Hill, 2007; Symmons et al., 2016). Therefore, the variability in limb phenotype in ZRS crispants may reflect subtle alteration of the *shh* expression rather than allele complexity or mosaicism in the founder. We speculate that low levels of *shh* signaling in ZPA stochastically affected digit number in regeneration. In addition, ZRS perturbation may also subtly alter spatio-temporal expression of *shh* and affect digit patterning (Shapiro et al., 2003). Intriguingly, even a few base deletions at the 17-bp snake-specific deletion site resulted in impaired limb regeneration, revealing that the small site (ZRS sgRNA2 targeting sequence) plays a crucial role in the reactivation of *shh*. This site contains predicted homeodomain DNA motifs, implying that the mutation disrupted Hox binding (Kvon et al., 2016; Leal and Cohn, 2016). To decipher the mechanism by which this site regulates *shh* expression during limb regeneration, further study is needed. We are also confident that this highly efficient gene knockout method will be suitable for evaluating regulatory elements in noncoding regions related to development and pathogenesis using salamanders.

Overall, in this study we demonstrated a highly efficient method of gene disruption for functional analysis of genes of interest and noncoding genome elements using Cas9 RNP in *P. waltl*. Recently, rapid advances of next-generation sequencing technology and assembly algorithms have enabled reading of the gigantic genome of salamanders (Elewa et al., 2017; Nowoshilow et al., 2018). Therefore, we expect that this reverse genetic tool will contribute to understanding the regenerative ability and other unique biological features of salamanders in the post-genome era.

4. Materials and methods

4.1. Animals

The Iberian ribbed newts (*Pleurodeles waltl*) used in this study were maintained in a closed colony following their original purchase from Tao (Chiba, Japan) in 2010. The animals were reared as described previously (Hayashi et al., 2013), unless stated otherwise. The developing stages were defined according to the criteria described by Shi and Boucaut (1995). For anesthesia before limb regeneration, MS-222 (Sigma, St. Louis, MO, USA) was used at a final concentration of 0.02%. Animal rearing and treatments were performed and approved in accordance with Guidelines for the Use and Care of Experimental Animals and the Institutional Animal Care and Use Committee of Hiroshima University and Tottori University.

4.2. Sequencing of ZRS locus and various genes

The ZRS locus of *P. waltl* was sequenced after inverse PCR cloning of this locus using the primers listed in Table S2. The partial genomic sequences and amplicon sequencing data of *tyr*, *pax6*, *tbx5*, and ZRS have been deposited in GenBank (LC378706) and the DDBJ Sequence Read Archive (DRA006550). The cDNA sequence for each gene was

predicted from the *P. waltl* transcriptome data set (Elewa et al., 2017) and resequenced (Fig. S1, 7).

4.3. Preparation of gRNAs

All gRNA targeting sequences are highlighted in Fig. S2. gRNAs were designed using CRISPR-direct (Naito et al., 2015). For sgRNA preparation, templates were assembled by a PCR-based strategy (Sakane et al., 2017). The oligonucleotide information is listed in Table S2. DNA templates were purified with a QIAquick PCR Purification Kit (Qiagen, Hilden, Germany); subsequently, sgRNAs were synthesized *in vitro* using a MEGA Shortscript T7 Kit and purified using a MEGA Clear Kit (Thermo Fisher Scientific, Waltham, MA, USA). The synthetic tracrRNA and crRNA were obtained from Integrated DNA Technologies (IDT; Skokie, IA, USA). The tracrRNA and crRNA were annealed in accordance with the manufacturer's instructions just before injection.

4.4. Microinjection

Microinjection was performed based on our previously reported protocols (Hayashi et al., 2014; Hayashi and Takeuchi, 2016; Sakane et al., 2017, 2018). A brief description of this protocol with minor modification is presented below. The fertilized eggs were treated with 0.5% cysteine in 0.25× Holtfreter's solution for 30 s to remove the jelly. De-jellied eggs were rinsed in 0.25× Holtfreter's solution and transferred into injection medium [4% Ficoll or 0.75% methylcellulose (Sigma) in 0.25× Holtfreter's solution]. The eggshells were removed using forceps and stored at 8 °C in injection medium until microinjection. One nanogram of recombinant Cas9 protein (Alt-R *S.p.* Cas9 Nuclease 3NLS; IDT) and 200 pg of sgRNA or 60 pg of crRNA + 160 pg of tracrRNA in 150 mM KCl and 20 mM HEPES buffer were injected into one-cell-stage embryos using Nanoject II (Drummond, Broomall, PA, USA). For targeting ZRS, 2 ng of Cas9 and 200 pg of each sgRNA (400 pg in total) were co-injected. After microinjection, the embryos were incubated overnight at 25 °C in injection medium and then transferred into 0.25× Holtfreter's solution. When injecting Cas9 + sgRNAs, 0.1× Marc's modified Ringer's (MMR) was used instead of 0.25× Holtfreter's solution and 5% Ficoll in 0.3× MMR was used as injection medium. Phenotypes were evaluated at 6 days postfertilization (dpf) for *tyr* disruption, and 9 dpf for *pax6* and *tbx5* disruption. Embryos that showed developmental defects from 2 dpf were here counted as having developmental defects.

4.5. Limb regeneration

Crispant or uninjected larvae were separated into single cases before the feeding stage and reared individually for one month. Larvae were anesthetized with 0.02% MS-222. Then, the left forelimbs were amputated with a surgical knife at the middle of the forearm level. Each amputated limb was stored at − 20 °C until genomic DNA extraction for amplicon sequencing. The number of digits was counted when uninjected control larvae completed regeneration, at 18 days postamputation (dpa). A small spike structure was not counted as representing a regenerating digit.

4.6. Genotyping

Genomic DNA was extracted from whole bodies of *tyr* (n = 5), *pax6* (n = 3), and amputated limb of ZRS crispants (n = 11) using DNeasy Blood and Tissue Kit (Qiagen), individually. Uninjected samples were also collected for each experimental group. An amplicon-sequencing library was prepared based on the Illumina "16S Metagenomic Sequencing Library Preparation." For the first round of PCR, the target regions containing gRNA targeting sites were amplified from individual genomic DNA of uninjected embryos, *tyr*, *pax6*, and ZRS crispants, using KOD FX Neo (TOYOBO, Osaka, Japan) with primer sets containing barcode and overhang adaptor sequences. Each PCR product was purified using a QIAquick PCR Purification Kit (Qiagen) and equal quantities of PCR products were pooled and re-purified using the same kit. For *tbx5* crispants (n = 3), the target region was amplified from the tail lysates using KAPA HiFi (Roche Diagnostics, Basel, Switzerland) with primer sets containing overhang adaptor sequences and purified using AMPure XP (Beckman Coulter, Pasadena, CA, USA). Then, each PCR product underwent the second round of PCR using different index primer sets. The second round of PCR was performed to construct a sequence library using a Nextra XT index kit (Illumina, San Diego, CA, USA). The final library was purified and sequenced on Illumina MiSeq. Library construction and sequencing were performed at the National Institute for Basic Biology (NIBB) and Microgen Japan (Kyoto, Japan). Amplicon-sequencing data were analyzed in accordance with the work of Sakane et al. (2018). PCR and Illumina sequence error rates were determined using uninjected samples, and then mutant reads were counted using an in-house script in R (version 3.3.3; for *tyr*, *pax6*, and ZRS) or CRISPResso (http://crispresso.rocks/; Pinello et al., 2016; for *tbx5*) (Table S1). For Sanger DNA sequencing of *tyr* F_1 larvae, amplicons were subcloned into pTA2 using Target Clone Plus (TOYOBO). Then, positive clones were selected by colony PCR and sequenced using BigDye Terminator v3.1 Cycle Sequencing kit (Life Technologies). All primers are listed in Table S2.

4.7. Histological analysis

Embryos were deeply anesthetized with 0.02% MS-222 and fixed with modified Carnoy's solution (65% ethanol, 30% formalin, 5% acetic acid). Tissues were processed for paraffin embedding and then sectioned at 8 μm. Sections were deparaffinized, rehydrated, and stained with hematoxylin and eosin.

4.8. VISTA global alignments

Comparison of *P. waltl* ZRS genomic sequences with other species was performed using the mVISTA program (Frazer et al., 2004; http://genome.lbl.gov/vista/) based on LAGAN multiple alignments (Brudno et al., 2003), using the default parameters. The genomic DNA sequences analyzed here are shown in Fig. S5.

4.9. RNA extraction and RT-qPCR

Forelimbs of crispant and uninjected larvae were amputated as described above, and then medium-bud-stage blastema (Iten and Bryant, 1973) was collected at 7 dpa. Tissues were incubated overnight in RNAlater (Thermo Fisher Scientific) at 4 °C, and stored at − 80 °C after removing the solution. Total RNA was isolated from each sample by using NucleoSpin RNA Plus XS with rDNase Set (TaKaRa Bio). The same amount of total RNA (20 ng) was reverse-transcribed and pre-amplified using CellAmp Whole Transcriptome Amplification Kit (TaKaRa Bio). qPCR was carried out by using SYBR Premix Ex Taq II (TaKaRa Bio) with a Step One real-time PCR system (Thermo Fisher Scientific). The copy numbers of each gene were quantified using pCRII-TOPO-Pw*shh* vector and purified PCR product of Pw*gapdh* as standards, and subsequently relative *shh* expression levels were normalized by *gapdh*. Two technical replicates were used per sample. All primers are listed in Table S2. Primer sets for qPCR were designed by Primer 3 (Untergasser et al., 2012). The statistical significance of differences was calculated by the Mann–Whitney *U*-test using EZR software (Kanda, 2013).

Acknowledgments

We thank Edanz Group (www.edanzediting.com/ac) for editing a draft of this manuscript and Mie Nakajima for helping microinjection.

This work was supported by Japan Society for the Promotion of Science (JSPS) KAKENHI Grant no. 15K06802 and 18K06257 (Grant-in-Aid for Scientific Research (C)) to K.T.S., Grant no. 16K08467 (Grant-in-Aid for Scientific Research (C)) to T.H., Grant no. 16H01254 (Grant-in-Aid for Scientific Research on Innovative Areas) to T.H., Grant no. 22124002 (Grant-in-Aid for Scientific Research on Innovative Areas) to K.A., Grant no. 16H04794 (Grant-in-Aid for Scientific Research (B)) to T.T., Grant no. 16H06376 (Grant-in-Aid for Scientific Research (S)) to K.A., and Grant no. 17J04796 (Grant-in-Aid for JSPS Fellows) to M.S. This work was also supported by NIBB Collaborative Research Program (18–204) to T.H.

Appendix A. Supporting information

Supplementary data associated with this article can be found in the online version at doi:10.1016/j.ydbio.2018.09.008.

References

Ablain, J., Durand, E.M., Yang, S., Zhou, Y., Zon, L.I., 2015. A CRISPR/Cas9 vector system for tissue-specific gene disruption in zebrafish. Dev. Cell 32, 756–764.
Agarwal, P., Wylie, J.N., Galceran, J., Arkhitko, O., Li, C., Deng, C., Grosschedl, R., Bruneau, B.G., 2003. Tbx5 is essential for forelimb bud initiation following patterning of the limb field in the mouse embryo. Development 130, 623–633.
Barbosa-Sabanero, K., Hoffmann, A., Judge, C., Lightcap, N., Tsonis, P.A., Del Rio-Tsonis, K., 2012. Lens and retina regeneration: new perspectives from model organisms. Biochem. J. 447, 321–334.
Brudno, M., Do, C.B., Cooper, G.M., Kim, M.F., Davydov, E., Green, E.D., Sidow, A., Batzoglou, S., Program, N.C.S., 2003. LAGAN and multi-LAGAN: efficient tools for large-scale multiple alignment of genomic DNA. Genome Res. 13, 721–731.
Bruneau, B.G., Nemer, G., Schmitt, J.P., Charron, F., Robitaille, L., Caron, S., Conner, D.A., Gessler, M., Nemer, M., Seidman, C.E., Seidman, J.G., 2001. A murine model of Holt-Oram syndrome defines roles of the T-box transcription factor Tbx5 in cardiogenesis and disease. Cell 106, 709–721.
Bryant, D.M., Johnson, K., DiTommaso, T., Tickle, T., Couger, M.B., Payzin-Dogru, D., Lee, T.J., Leigh, N.D., Kuo, T.H., Davis, F.G., Bateman, J., Bryant, S., Guzikowski, A.R., Tsai, S.L., Coyne, S., Ye, W.W., Freeman, R.M., Peshkin, L., Tabin, C.J., Regev, A., Haas, B.J., Whited, J.L., 2017. A tissue-mapped axolotl de novo transcriptome enables Identification of limb regeneration factors. Cell Rep. 18, 762–776.
Burger, A., Lindsay, H., Felker, A., Hess, C., Anders, C., Chiavacci, E., Zaugg, J., Weber, L.M., Catena, R., Jinek, M., Robinson, M.D., Mosimann, C., 2016. Maximizing mutagenesis with solubilized CRISPR-Cas9 ribonucleoprotein complexes. Development 143, 2025–2037.
Elewa, A., Wang, H., Talavera-López, C., Joven, A., Brito, G., Kumar, A., Hameed, L.S., Penrad-Mobayed, M., Yao, Z., Zamani, N., Abbas, Y., Abdullayev, I., Sandberg, R., Grabherr, M., Andersson, B., Simon, A., 2017. Reading and editing the Pleurodeles waltl genome reveals novel features of tetrapod regeneration. Nat. Commun. 8, 2286.
Fei, J.F., Schuez, M., Tazaki, A., Taniguchi, Y., Roensch, K., Tanaka, E.M., 2014. CRISPR-mediated genomic deletion of Sox2 in the axolotl shows a requirement in spinal cord neural stem cell amplification during tail regeneration. Stem Cell Rep. 3, 444–459.
Flament, S., Dumond, H., Chardard, D., Chesnel, A., 2009. Lifelong testicular differentiation in Pleurodeles waltl (Amphibia, Caudata). Reprod. Biol. Endocrinol. 7, 21.
Flowers, G.P., Timberlake, A.T., McLean, K.C., Monaghan, J.R., Crews, C.M., 2014. Highly efficient targeted mutagenesis in axolotl using Cas9 RNA-guided nuclease. Development 141, 2165–2171.
Frazer, K.A., Pachter, L., Poliakov, A., Rubin, E.M., Dubchak, I., 2004. VISTA: computational tools for comparative genomics. Nucleic Acids Res. 32, W273–W279.
Garrity, D.M., Childs, S., Fishman, M.C., 2002. The heartstrings mutation in zebrafish causes heart/fin Tbx5 deficiency syndrome. Development 129, 4635–4645.
Han, Y., Slivano, O.J., Christie, C.K., Cheng, A.W., Miano, J.M., 2015. CRISPR-Cas9 genome editing of a single regulatory element nearly abolishes target gene expression in mice–brief report. Arterioscler. Thromb. Vasc. Biol. 35, 312–315.
Hayashi, T., Sakamoto, K., Sakuma, T., Yokotani, N., Inoue, T., Kawaguchi, E., Agata, K., Yamamoto, T., Takeuchi, T., 2014. Transcription activator-like effector nucleases efficiently disrupt the target gene in Iberian ribbed newts (Pleurodeles waltl), an experimental model animal for regeneration. Dev. Growth Differ. 56, 115–121.
Hayashi, T., Takeuchi, T., 2016. Mutagenesis in newts: protocol for Iberian ribbed newts. Methods Mol. Biol. 1338, 119–126.
Hayashi, T., Yokotani, N., Tane, S., Matsumoto, A., Myouga, A., Okamoto, M., Takeuchi, T., 2013. Molecular genetic system for regenerative studies using newts. Dev. Growth Differ. 55, 229–236.
Hill, R.E., 2007. How to make a zone of polarizing activity: insights into limb development via the abnormality preaxial polydactyly. Dev. Growth Differ. 49, 439–448.
Inoue, T., Inoue, R., Tsutsumi, R., Tada, K., Urata, Y., Michibayashi, C., Takemura, S., Agata, K., 2012. Lens regenerates by means of similar processes and timeline in adults and larvae of the newt Cynops pyrrhogaster. Dev. Dyn. 241, 1575–1583.
Iten, L.E., Bryant, S.V., 1973. Forelimb regeneration from different levels of amputation in the newt, Notophthalmus viridescens: length, rate, and stages. Wilhelm. Roux Arch. Entwickl. Mech. Org. 173, 263–282.
Kanda, Y., 2013. Investigation of the freely available easy-to-use software 'EZR' for medical statistics. Bone Marrow Transplant. 48, 452–458.
Kim, S., Kim, D., Cho, S.W., Kim, J., Kim, J.S., 2014. Highly efficient RNA-guided genome editing in human cells via delivery of purified Cas9 ribonucleoproteins. Genome Res. 24, 1012–1019.
Kuscu, C., Arslan, S., Singh, R., Thorpe, J., Adli, M., 2014. Genome-wide analysis reveals characteristics of off-target sites bound by the Cas9 endonuclease. Nat. Biotechnol. 32, 677–683.
Kvon, E.Z., Kamneva, O.K., Melo, U.S., Barozzi, I., Osterwalder, M., Mannion, B.J., Tissières, V., Pickle, C.S., Plajzer-Frick, I., Lee, E.A., Kato, M., Garvin, T.H., Akiyama, J.A., Afzal, V., Lopez-Rios, J., Rubin, E.M., Dickel, D.E., Pennacchio, L.A., Visel, A., 2016. Progressive loss of function in a limb enhancer during snake evolution. Cell 167, 633–642, (e611).
Leal, F., Cohn, M.J., 2016. Loss and re-emergence of legs in snakes by modular evolution of sonic hedgehog and HOXD enhancers. Curr. Biol. 26, 2966–2973.
Leone, M., Magadum, A., Engel, F.B., 2015. Cardiomyocyte proliferation in cardiac development and regeneration: a guide to methodologies and interpretations. Am. J. Physiol. Heart Circ. Physiol. 309, H1237–H1250.
Lettice, L.A., Devenney, P., De Angelis, C., Hill, R.E., 2017. The conserved Sonic Hedgehog limb enhancer consists of discrete functional elements that regulate precise spatial expression. Cell Rep. 20, 1396–1408.
Lettice, L.A., Williamson, I., Devenney, P.S., Kilanowski, F., Dorin, J., Hill, R.E., 2014. Development of five digits is controlled by a bipartite long-range cis-regulator. Development 141, 1715–1725.
Naito, Y., Hino, K., Bono, H., Ui-Tei, K., 2015. CRISPRdirect: software for designing CRISPR/Cas guide RNA with reduced off-target sites. Bioinformatics 31, 1120–1123.
Nowoshilow, S., Schloissnig, S., Fei, J.F., Dahl, A., Pang, A.W.C., Pippel, M., Winkler, S., Hastie, A.R., Young, G., Roscito, J.G., Falcon, F., Knapp, D., Powell, S., Cruz, A., Cao, H., Habermann, B., Hiller, M., Tanaka, E.M., Myers, E.W., 2018. The axolotl genome and the evolution of key tissue formation regulators. Nature.
Oviedo, N.J., Beane, W.S., 2009. Regeneration: the origin of cancer or a possible cure? Semin. Cell Dev. Biol. 20, 557–564.
Parish, C.L., Beljajeva, A., Arenas, E., Simon, A., 2007. Midbrain dopaminergic neurogenesis and behavioural recovery in a salamander lesion-induced regeneration model. Development 134, 2881–2887.
Pinello, L., Canver, M.C., Hoban, M.D., Orkin, S.H., Kohn, D.B., Bauer, D.E., Yuan, G.C., 2016. Analyzing CRISPR genome-editing experiments with CRISPResso. Nat. Biotechnol. 34, 695–697.
Rallis, C., Bruneau, B.G., Del Buono, J., Seidman, C.E., Seidman, J.G., Nissim, S., Tabin, C.J., Logan, M.P., 2003. Tbx5 is required for forelimb bud formation and continued outgrowth. Development 130, 2741–2751.
Ran, F.A., Hsu, P.D., Lin, C.Y., Gootenberg, J.S., Konermann, S., Trevino, A.E., Scott, D.A., Inoue, A., Matoba, S., Zhang, Y., Zhang, F., 2013. Double nicking by RNA-guided CRISPR Cas9 for enhanced genome editing specificity. Cell 154, 1380–1389.
Roy, S., Gardiner, D.M., 2002. Cyclopamine induces digit loss in regenerating axolotl limbs. J. Exp. Zool. 293, 186–190.
Sagai, T., Hosoya, M., Mizushina, Y., Tamura, M., Shiroishi, T., 2005. Elimination of a long-range cis-regulatory module causes complete loss of limb-specific Shh expression and truncation of the mouse limb. Development 132, 797–803.
Sakane, Y., Iida, M., Hasebe, T., Fujii, S., Buchholz, D.R., Ishizuya-Oka, A., Yamamoto, T., Suzuki, K.T., 2018. Functional analysis of thyroid hormone receptor beta in Xenopus tropicalis founders using CRISPR-Cas. Biol. Open, 7.
Sakane, Y., Suzuki, K.T., Yamamoto, T., 2017. A simple protocol for loss-of-function analysis in Xenopus tropicalis founders using the CRISPR-Cas system. Methods Mol. Biol. 1630, 189–203.
Seilern-Aspang, F., Kratochwil, K., 1962. Induction and differentiation of an epithelial tumour in the newt (Triturus cristatus). J. Embryol. Exp. Morphol. 10, 337–356.
Shapiro, M.D., Hanken, J., Rosenthal, N., 2003. Developmental basis of evolutionary digit loss in the Australian lizard Hemiergis. J. Exp. Zool. B Mol. Dev. Evol. 297, 48–56.
Shi, D.L., Boucaut, J.C., 1995. The chronological development of the urodele amphibian Pleurodeles waltl (Michah). Int. J. Dev. Biol. 39, 427–441.
Shigeta, M., Sakane, Y., Iida, M., Suzuki, M., Kashiwagi, K., Kashiwagi, A., Fujii, S., Yamamoto, T., Suzuki, K.T., 2016. Rapid and efficient analysis of gene function using CRISPR-Cas9 in Xenopus tropicalis founders. Genes Cells 21, 755–771.
Shin, H.Y., Wang, C., Lee, H.K., Yoo, K.H., Zeng, X., Kuhns, T., Yang, C.M., Mohr, T., Liu, C., Hennighausen, L., 2017. CRISPR/Cas9 targeting events cause complex deletions and insertions at 17 sites in the mouse genome. Nat. Commun. 8, 15464.
Stocum, D.L., 2017. Mechanisms of urodele limb regeneration. Regeneration 4, 159–200.
Suzuki, K.T., Isoyama, Y., Kashiwagi, K., Sakuma, T., Ochiai, H., Sakamoto, N., Furuno, N., Kashiwagi, A., Yamamoto, T., 2013. High efficiency TALENs enable F0 functional analysis by targeted gene disruption in Xenopus laevis embryos. Biol. Open 2, 448–452.
Symmons, O., Pan, L., Remeseiro, S., Aktas, T., Klein, F., Huber, W., Spitz, F., 2016. The Shh topological domain facilitates the action of remote enhancers by reducing the effects of genomic distances. Dev. Cell 39, 529–543.
Tsutsumi, R., Inoue, T., Yamada, S., Agata, K., 2015. Reintegration of the regenerated and the remaining tissues during joint regeneration in the newt Cynops pyrrhogaster. Regeneration 2, 26–36.
Untergasser, A., Cutcutache, I., Koressaar, T., Ye, J., Faircloth, B.C., Remm, M., Rozen, S.G., 2012. Primer3–new capabilities and interfaces. Nucleic Acids Res. 40, e115.
Urata, Y., Yamashita, W., Inoue, T., Agata, K., 2018. Spatio-temporal neural stem cell behavior leads to both perfect and imperfect structural brain regeneration in adult newts. Biol. Open, 7.

Williamson, I., Hill, R.E., Bickmore, W.A., 2011. Enhancers: from developmental genetics to the genetics of common human disease. Dev. Cell 21, 17–19.
Wu, X., Scott, D.A., Kriz, A.J., Chiu, A.C., Hsu, P.D., Dadon, D.B., Cheng, A.W., Trevino, A.E., Konermann, S., Chen, S., Jaenisch, R., Zhang, F., Sharp, P.A., 2014. Genome-wide binding of the CRISPR endonuclease Cas9 in mammalian cells. Nat. Biotechnol. 32, 670–676.
Yasue, A., Kono, H., Habuta, M., Bando, T., Sato, K., Inoue, J., Oyadomari, S., Noji, S., Tanaka, E., Ohuchi, H., 2017. Relationship between somatic mosaicism of Pax6 mutation and variable developmental eye abnormalities-an analysis of CRISPR genome-edited mouse embryos. Sci. Rep. 7 (53).
Zhu, X., Xu, Y., Yu, S., Lu, L., Ding, M., Cheng, J., Song, G., Gao, X., Yao, L., Fan, D., Meng, S., Zhang, X., Hu, S., Tian, Y., 2014. An efficient genotyping method for genome-modified animals and human cells generated with CRISPR/Cas9 system. Sci. Rep. 4, 6420.
Zuo, E., Cai, Y.J., Li, K., Wei, Y., Wang, B.A., Sun, Y., Liu, Z., Liu, J., Hu, X., Wei, W., Huo, X., Shi, L., Tang, C., Liang, D., Wang, Y., Nie, Y.H., Zhang, C.C., Yao, X., Wang, X., Zhou, C., Ying, W., Wang, Q., Chen, R.C., Shen, Q., Xu, G.L., Li, J., Sun, Q., Xiong, Z.Q., Yang, H., 2017. One-step generation of complete gene knockout mice and monkeys by CRISPR/Cas9-mediated gene editing with multiple sgRNAs. Cell Res. 27, 933–945.